SCIENTIFIC REPORTS

OPEN

Large low field magnetocaloric effect in first-order phase transition compound TlFe$_3$Te$_3$ with low-level hysteresis

Qianhui Mao[1], Jinhu Yang[2], Hangdong Wang[1,2], Rajwali Khan[1], Jianhua Du[1], Yuxing Zhou[1], Binjie Xu[1], Qin Chen[1] & Minghu Fang[1,3]

Magnetic refrigeration based on the magnetocaloric effect (MCE) is an environment-friendly, high-efficiency technology. It has been believed that a large MCE can be realized in the materials with a first-order magnetic transition (FOMT). Here, we found that TlFe$_3$Te$_3$ is a ferromagnetic metal with a first-order magnetic transition occurring at Curie temperature $T_C = 220$ K. The maximum values of magnetic entropy change (ΔS_M^{max}) along the crystallographic c-axis, estimated from the magnetization data, reach to 5.9 J kg^{-1}K^{-1} and 7.0 J kg^{-1} K^{-1} for the magnetic field changes, $\Delta H = 0$–1 T and 0–2 T, respectively, which is significantly larger than that of MCE materials with a second-order magnetic transition (SOMT). Besides the large ΔS_M, the low-level both thermal and field hysteresis make TlFe$_3$Te$_3$ compound an attractive candidate for magnetic refrigeration. Our findings should inspire the exploration of high performance new MCE materials.

Magnetic refrigeration based on MCE is an environment-friendly, high-efficiency technology compared to the traditional gas-cycle refrigeration[1–4]. After the discovery of the first magnetic refrigeration prototype near room temperature[5] and the giant MCE in Gd$_5$(Si$_2$Ge$_2$)[6,7], a large MCE has been realized in a lot of materials in the past two decades, such as ReCo$_2$ (Re = Er, Ho, and Dy) alloys[8,9], manganite oxides (Re, M)MnO$_3$ (Re = Lanthanide, M = Ca, Sr, and Ba)[10,11], Ni-Mn-X (X = Ga, In, and Sn) based Heusler alloys[12–16], MnAs based compounds[3,17–19], La(Fe, Si)$_{13}$ and related compounds[20–23], as well as rare earth based intermetallic compounds[24–30]. Amongst the families of MCE materials, the compounds with first-order magnetic transition (FOMT) have been found promising due to their large and/or sharp changes in magnetization and the strong coupling between crystallographic structure and magnetism, such as Gd$_5$Ge$_{4-x}$Si$_x$[7], MnAs$_{1-x}$Sb$_x$[18,31], MnFe(As, P, Si, Ge)[17,32], LaFe$_{13-x}$Si$_x$(H$_\delta$)[14,21,23] and Heusler-type magnetic shape-memory alloys[14,16]. However, in these materials, the magnetic transitions are frequently accompanied by significant thermal and/or magnetic hysteresis, which would limit the life span of refrigerants or even make the refrigeration cycle impossible[3,33]. In order to reduce or even eliminate the magnetic hysteresis losses, there have been two strategies. One is to treat the giant MCE materials by special methods, such as microstructure-tuning, as porosity[34], fragmentation[35–37], melt-spun[38–40], or chemical tuning, as doping[41]. Another is to search for new high performance compounds with SOMT[42]. However, the performances in materials with SOMT are rather modest when compared with that with FOMT. It is therefore interesting to search for new FOMT materials with low-level hysteresis and without any additional treatments.

The crystal structure and physical properties of TlFe$_3$Te$_3$ were reported by two groups in 1984[43,44]. TlFe$_3$Te$_3$ crystalizes in a hexagonal structure with space group P6$_3$/m, which consists of one-dimensional metallic cluster |Fe$_3$Te$_3$|$_\infty$ chains along the hexagonal c-axis, separated by the parallel chains of Tl atoms (see Fig. 1). The authors concluded that the compound undergoes a first-order transition from paramagnetic to ferromagnetic at 220 K based on their physical property measurements. However, neither of them observed discernible thermal and field hysteresis. Since the absence of hysteresis is appealing for magnetic refrigerant, in this report, we recheck the type of the magnetic transition and elucidate the MCE of TlFe$_3$Te$_3$ by performing resistivity and magnetization

[1]Department of Physics, Zhejiang University, Hangzhou 310027, China. [2]Department of Physics, Hangzhou Normal University, Hangzhou 310036, China. [3]Collaborative Innovation Center of Advanced Microstructures, Nanjing 210093, China. Correspondence and requests for materials should be addressed to M.F. (email: mhfang@zju.edu.cn)
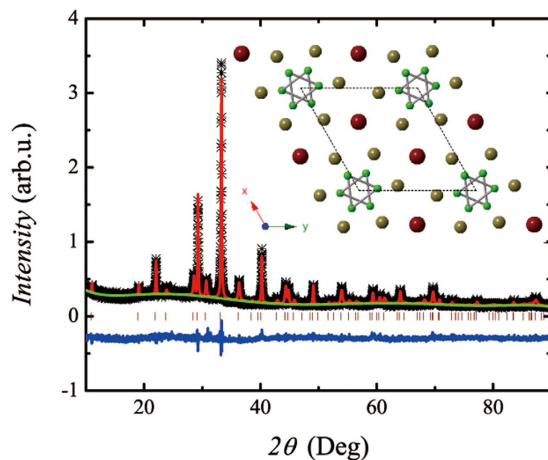
Figure 1. The powder X-ray diffraction (XRD) pattern (black star: observed data; red line: calculated curve; green line: background; blue line: difference; wine bar: Bragg positions) and the crystal structure of TlFe$_3$Te$_3$ viewed along c-axis (red ball: Tl; dark yellow ball: Te; green ball: Fe).

measurements. We found that this compound exhibits a large MCE with a small magnetic field change, ΔH, and with a low-level thermal and field hysteresis, thus identifying it to be another class of solids for the magnetic refrigerants.

Results and Discussion

Figure 1 presents the powder x-ray diffraction (XRD) pattern of TlFe$_3$Te$_3$ and its Rietveld refinement. All the diffraction peaks could be indexed by a hexagonal structure with space group P6$_3$/m. The lattice parameters $a = 9.355(1)$ Å and $c = 4.224(5)$ Å were obtained by the refinement, which are in good agreement with previous reports[44]. The electron probe micro-analyzer (EPMA) experiments performed on several single crystals verified that the sample composition (the average atomic ratio) is of Tl : Fe : Te = 0.99(1) : 2.95(2) : 3.00(1), which is in consistent with the nominal composition. The temperature dependence of electrical resistivity along c-axis, $\rho(T)$, for a TlFe$_3$Te$_3$ crystal is shown in Fig. 2(a). In the whole measuring temperature range, the positive resistivity-temperature coefficient of $\rho(T)$ indicates its metallic behavior. The resistivity has a very sharp drop at 220 K with detectable thermal hysteresis [see the inset of Fig. 2(a)], which is associated with the first-order ferromagnetic transition. The resistivity at 300 K and 1.8 K are of 120 $\mu\Omega$ cm and 1.8 $\mu\Omega$ cm, respectively. The small resistivity should be viewed as a merit since a good thermal conductivity is required for a high performance magnetic refrigerant material[45]. Both a rather low residual resistivity and a considerable large residual resistivity ratio $(RRR) = 67$ indicate that our crystals are of high quality.

Figure 2(b) shows the magnetization as a function of temperature, $M(T)$, measured from 2 to 300 K in an applied magnetic field $H = 1000$ Oe, aligned both $\parallel$ and $\perp$ the c-axis, with a field cooling process. A sharp increase of M for both directions at the Curie temperature, $T_C \sim 220$ K, confirms the occurrence of a ferromagnetic transition. Larger magnetization along c-axis suggests that the easy axis of magnetization is in the c axis. As discussed by Uhl et $al.$[43] and Pelizzone et $al.$[44], the strong magnetic anisotropy observed in the ferromagnetic state is certainly related to its peculiar structure being composed of $|Fe_3Te_3|_\infty$ chains, whose central part is a column of edge-sharing octahedral Fe clusters. The Fe-Fe distance of 2.6 Å within the clusters are comparable to the interatomic distance in metallic iron, while the nearest two Fe atoms belong to different $|Fe_3Te_3|_\infty$ chains are 6.7 Å apart. Thus, a strong anisotropy of the exchange coupling is to be expected. As shown in Fig. 2(c,d), it is clear that the $M(T)$ curves near T_C exhibit a small thermal hysteresis for both directions, which is in contrast to that reported by Uhl et $al.$[43] and Pelizzone et $al.$[44], who did not observe any hysteresis in their measurements. We observed a distinguishable but very small hysteresis, ($i.e.$, the hysteresis temperature $\Delta T_{hy} = 0.2$ K for $H \parallel c$-axis and 0.1 K for $H \perp c$-axis), which suggests that a first-order ferromagnetic transition occurs at $\sim$220 K.

In order to further identify the type of the transition and to explore the MCE, we performed the isothermal magnetization measurements near the T_C. Figure 3 shows the magnetization as a function of magnetic field, $M(H)$, measured at various temperatures around T_C with both $H \parallel c$-axis and $H \perp c$-axis, and with both increasing and decreasing magnetic field. A small magnetic hysteresis was again observed. The maximum hysteresis is 50 Oe for $H \parallel c$-axis [see Fig. 3(a)], while for $H \perp c$-axis, the hysteresis is rather small and becomes even indiscernible [see Fig. 3(b)]. The $M(H)$ curves for both $H \parallel c$-axis and $H \perp c$-axis exhibit a different behavior, which is associated with the large anisotropy of magnetization discussed above. The M^2 versus H/M curves for both directions are shown in Fig. 3(c,d), respectively. According to the Banerjee criterion[46], the curves at some temperatures have a negative slope and a inflection, which confirms further the occurrence of the first-order ferromagnetic transition around 220 K. The small hysteresis in $M(H)$ curves enables us to use the Maxwell equation to estimate the isothermal magnetic entropy change (ΔS_M). The ΔS_M is calculated by a formula:

$$\Delta S_M(T,\,\Delta H) = \sum_0^{max} \frac{M_i - M_{i-1}}{T_i - T_{i-1}} \Delta H$$

(1)

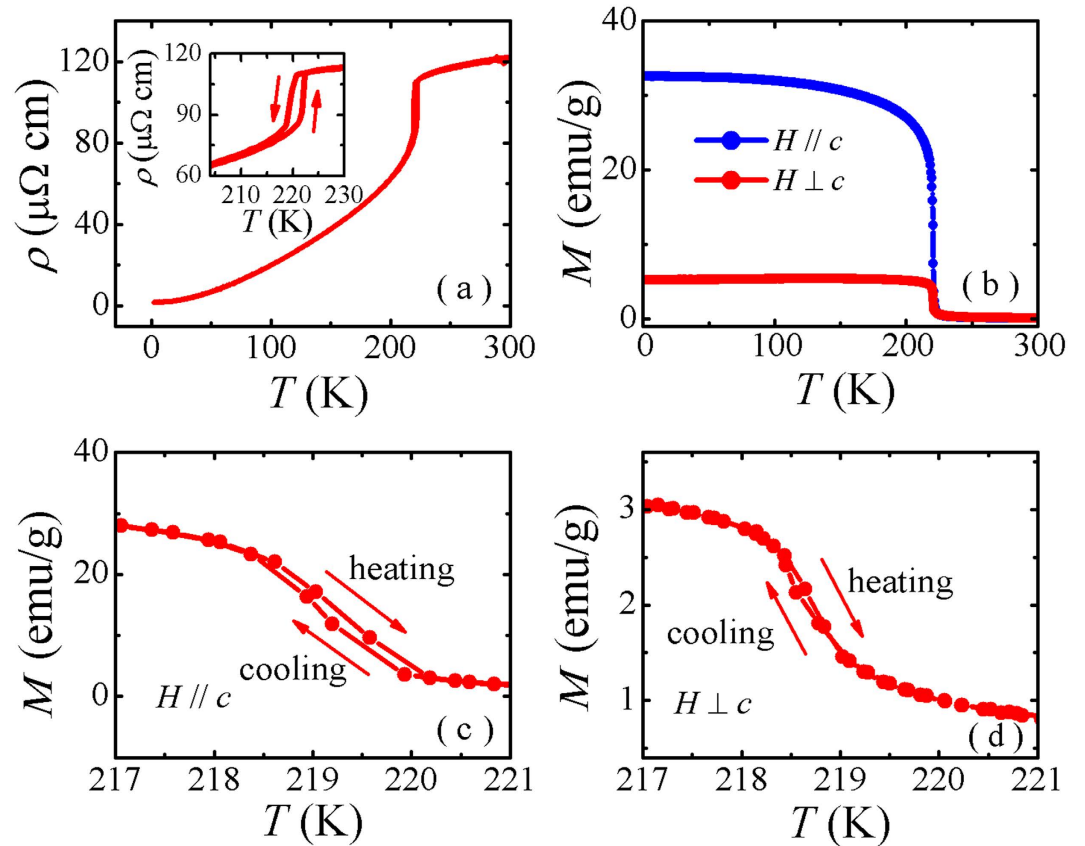**Figure 2.** (**a**) The temperature dependence of resistivity with a current applied parallel to c-axis and the expansion near the transition temperature (inset). (**b**) The temperature dependence of magnetization, $M(T)$, for both $H\|c$-axis and $H\perp c$-axis. The $M(T)$ near the transition temperature for (**c**) $H\|c$-axis, (**d**) $H\perp c$-axis, the arrows show the cooling and heating process during measurements.

which is an approximation of the integral form of the Maxwell equation.

$$\Delta S_M(T,\,\Delta H) = \int_0^H \left(\frac{\partial M}{\partial T}\right) dH \tag{2}$$

Figure 4(a,b) present the temperature dependence of $-\Delta S_M$ with the magnetic field changes ΔH up to 0–5 T, for both $H\|c$-axis and $H\perp c$-axis. For $H\|c$-axis, the $-\Delta S_M(T)$ curve with $\Delta H = 0$–1 T shows a pronounced peak around T_C, and a table-like behavior can be observed in the $-\Delta S_M(T)$ curves with $\Delta H = 0$–2 T and 0–3 T, *i.e.*, there is a temperature range corresponding to the maximum value of magnetic entropy change, which is beneficial for application. With $\Delta H = 0$–1, 0–2, 0–3, 0–4, and 0–5 T, $-\Delta S_M^{max} = 5.9$, 7.0, 8.2, 8.5 and 8.9 J/kg K, respectively, which increases continuously with the increasing field change and tends to almost saturate at higher magnetic field change. It is known that a "table-like" behavior and no strong ΔH dependence of $-\Delta S_M^{max}$ value are the typical behaviors for FOMT materials[2,45]. Although $-\Delta S_M^{max}$ values are smaller than that for the some giant MCE materials (see Table 1), these values of TlFe$_3$Te$_3$ are comparable with the most potential magnetic refrigerant materials with the a first-order ferromagnetic transition (see Table 1). For the $H\perp c$-axis case, all the $-\Delta S_M(T)$ curves with different ΔH values exhibit a peak around T_C without table-like behavior, and the maximum value of magnetic entropy change $-\Delta S_M^{max}$ is smaller than that for the $H\|c$-axis. The anisotropy of MCE may origin from the peculiar magnetic structure, as discussed above.

Another important quality factor of magnetic refrigerant materials is the relative cooling power (RCP) or/and refrigeration capacity (RC), defined[29] usually as the product of $-\Delta S_M^{max}$ and the full width at half maximum in the $-\Delta S_M(T)$ curve, as an example, *i.e.*, $T_{hot} - T_{cold}$ for $\Delta H = 0$–1 T in Fig. 4(a). RCP/RC is a measurement of the amount of heat transfer between the cold and hot reservoirs in an ideal refrigeration cycle. Due to the limitation of data measured in our experiments, we only estimated that the RCP values for the $\Delta H = 0$–1, 0–2 and 0–3 T, are of 13, 50, and 74.6 J/kg, respectively. Recently, as a figure of merit for the magnetic refrigerant materials, the dimensionless materials efficiency[47,48], $\eta = |Q/W|$, is taken into consideration, where electrical or mechanical work, W, is done to drive highly reversible caloric effects in an isothermal body, whose entropy is thus modified such that heat, Q, flows to ($Q < 0$) or from ($Q > 0$). Here, we estimated the mass-normalized values of $|W|$ by integrating $-\mu_0 M dH_0$ from the $M(H_0)$ data at T_C, and evaluated the mass-normalized value of heat Q by integrating $\mu_0 T_0 (\partial M/\partial T)_H$ with respect to H from the $M(H_0)$ data at T_C, which follows from the Maxwell relation
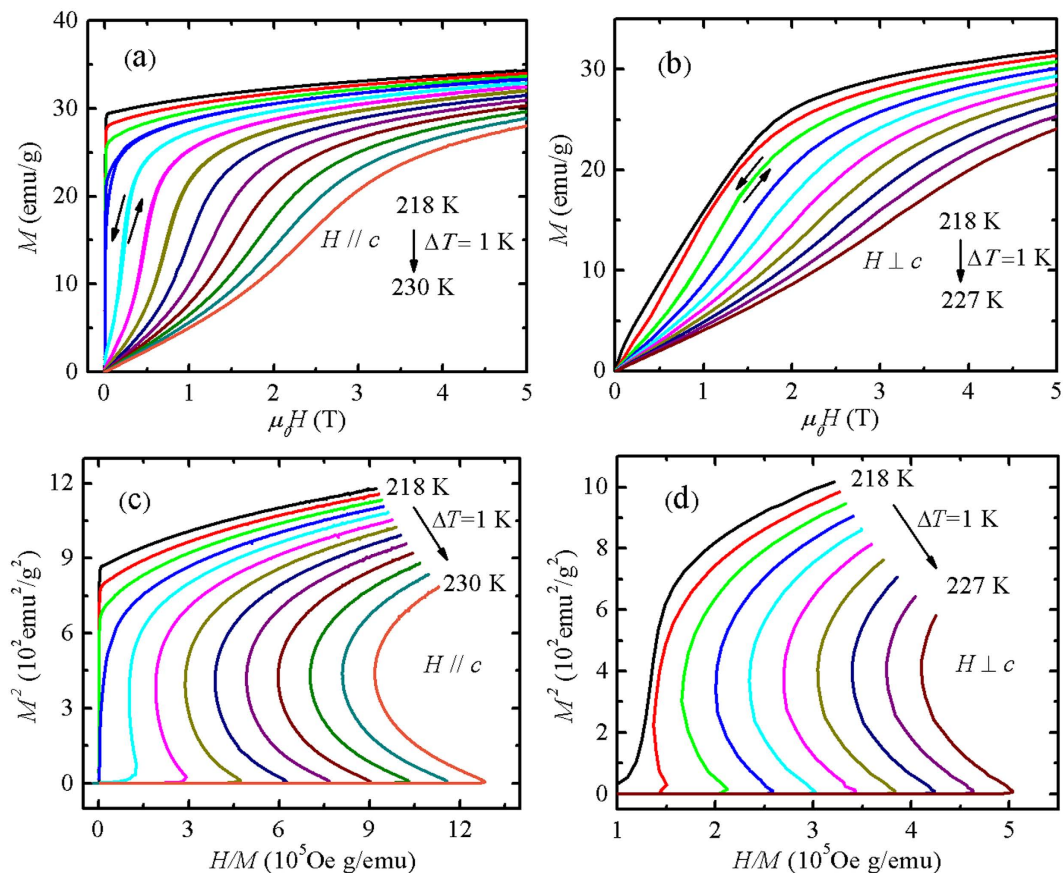
Figure 3. The isothermal magnetization near T_C as a function of magnetic field, $M(H)$, measured with a temperature step of 1 K for H (**a**) $\parallel$ and (**b**) $\perp$ the c axis. The arrows indicate the measurements with increasing and decreasing magnetic field process. The corresponding M^2 vs H/M curves for H (**c**) $\parallel$ and (**d**) $\perp$ the c axis.
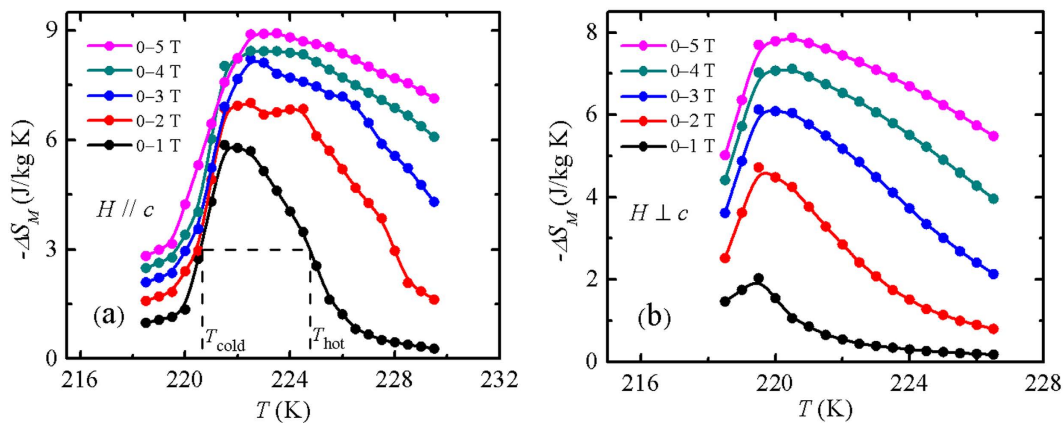

Figure 4. The magnetic entropy change as a function of temperature, $-\Delta S_M(T)$, around T_C, with the different field change $\Delta H = 0$–1, 0–2, 0–3, 0–4, and 0–5 T for H (**a**) $\parallel$ and (**b**) $\perp$ the c axis. $T_{hot} - T_{cold}$ in (**a**) represents the full width at half maximum in $-\Delta S_M(T)$ curve for $\Delta H = 0$–1 T.

$\mu_0(\partial M/\partial T)_H = (\partial S/\partial H)_T$. The materials efficiency η values at T_C was estimated to be of 65.7, 32.0, 23.2, 17.1, and 13.9 for $\Delta H = 0$–1, 0–2, 0–3, 0–4, and 0–5 T, respectively.

As a comparison of MCE properties, we choose several compounds with a similar magnetic transition temperature, T_M, as well as some typical materials with a near room temperature, T_M, focusing on the performance under $\Delta H = 0$–2 T (the maximum magnetic field generated by a permanent magnet is about 2 T). As listed in Table 1, although the $-\Delta S_M^{max}$ of TlFe$_3$Te$_3$ is less than that in the some pronounced materials with FOMT, such as GdSi$_2$Ge$_2$, MnFeP$_{0.45}$As$_{0.55}$, LaFe$_{11.7}$Si$_{1.3}$ and 20-LaFe$_{11.57}$Si$_{1.43}$ materials, $-\Delta S_M^{max}$ of TlFe$_3$Te$_3$ is significantly larger

Sample	T_M	$-\Delta S_M^{max}$ (0–2 T)	Δ^{Thy}	RCP (0–2 T)	η (0–2 T)	Transition type	Ref.
$TlFe_3Te_3$	220	7.02	0.2	50.4	32.0	FOMT	This work
$TbCo_2$	231	3.52	0	82.7	11.0	SOMT	49
$Gd_2In_{0.8}Al_{0.2}$	198	3.0	0	31.2	7.29	SOMT	50
Tb_5Si_4	225	5.2	0	205.4	—	SOMT	51
$LaFe_{11}(Si_{0.5}Al_{0.5})_2$	213	3.7	0	—	8.1	SOMT	52
$Ni_{50}Mn_{34}In_{16}$	190	9.5	~8	93.1	36.6	FOMT	48, 53
$LaFe_{11.7}Si_{1.3}$	184	28	~1	540	37.6–50	FOMT	48
20-$LaFe_{11.57}Si_{1.43}$	198	11.1	3	66.8	23.4	FOMT	39
40-$LaFe_{11.57}Si_{1.43}$	210	5.4	0.4	60.2	7.8	FOMT	39
$GdSi_2Ge_2$	276	14	2–14	142	27.2	FOMT	6, 48
$MnFeP_{0.45}As_{0.55}$	308	14.5	>1	150	96.7	FOMT	17, 48
$Ni_{50}Mn_{37}Sn_{13}$	299	6.9	—	96.6	66.8	FOMT	48, 54

Table 1. Comparison of the MCE properties with some representative materials with a similar magnetic transition temperature. The 20-$LaFe_{11.57}Si_{1.43}$ and 40-$LaFe_{11.57}Si_{1.43}$ represents the ribbon samples prepared at 20 m/s and 40 m/s rates, respectively. The units of T_M and ΔT_{hy} are Kelvin (K), ΔS_M^{max} is J/kg K, RCP is J/kg.

than that with SOMT. Both the RCP and η values of $TlFe_3Te_3$ are comparable with the most MEC materials, except for some special compounds, such as Tb_5Si_4, $LaFe_{11.7}Si_{1.3}$, $GdSi_2Ge_2$ and $MnFeP_{0.45}As_{0.55}$. Besides having a larger ΔS_M, $TlFe_3Te_3$ has some other advantages, such as a rare-earth-free element, a low synthesis temperature, as well as a low-level hysteresis in the as-grown crystals. But it should be pointed out that the toxicity of Tl element is not so good for the commercial utilization, which may be improved by the replacement of In, Ba, K for Tl in the future.

In summary, after successfully growing $TlFe_3Te_3$ single crystals, we carried systematically out the measurements of its resistivity and magnetization to investigate the nature of the magnetic phase transition and the MCE. It was found that $TlFe_3Te_3$ is a FOMT metal with $T_C = 220$ K and has a small thermal and field hysteresis near T_C. The relative large MCE at a low ΔH makes this compound a promising candidate for magnetic refrigeration around 220 K. Further efforts should be done to substitute Tl by other nontoxic elements in order to utilize this type of materials widely.

Methods

Single crystals of $TlFe_3Te_3$ were grown using a self-flux method. A mixture with a ratio of Tl:Fe:Te = 1:3:3 was placed in an alumina crucible, sealed in an evacuated quartz tube, heated at 923 K for 5 days. The product was a black powder from which needle-like single crystals with a typical dimension of ~$0.4 \times 0.4 \times 4$ mm^3 could be isolated. Powder XRD measurements on crushed single crystals were carried out at room temperature on a PANalytical x-ray diffractometer (Model EMPYREAN) with a monochromatic Cu $K_{\alpha 1}$ radiation to identify the phase purity and the crystal structure. The composition was confirmed by an electron probe micro-analyzer (EPMA) (Jeol JXA-8100). The magnetic measurements were performed on a Quantum Design Magnetic Property Measurement System (SQUID-VSM, MPMS-5) and the resistivity measurements were carried out on a Physical Property Measurement System (PPMS-9).

References

1. Gschneidner Jr, K. A., Pecharsky, V. K. & Tsokol A. O. Recent developments in magnetocaloric materials. *Rep. Prog. Phys.* **68,** 1479–1539 (2005).
2. Gschneidner Jr, K. A. & Pecharsky, V. K. Magnetocaloric materials. *Annu. Rev. Mater. Sci.* **30,** 387 (2000).
3. Brück, E. Developments of magnetocaloric refrigeration. *J. Phys. D: Appl. Phys.* **38,** R381 (2005).
4. Smith, A. *et al.* Materials challenges for high performance magnetocaloric refrigeration devices. *Adv. Energy Mater.* **2,** 1288 (2012).
5. Zimm, C. *et al.* Description and performance of a near-toom temperature magnetic refrigerator. *Adv. Cryog. Eng.* **43,** 1759 (1998).
6. Pecharsky, V. K. & Gschneidner Jr, K. A. Giant magnetocaloric effect in Gd$_5$(Si$_2$Ge$_2$). *Phys. Rev. Lett.* **78,** 4494 (1997).
7. Pecharsky, V. K. & Gschneidner Jr, K. A. Tunable magnetic regenerator alloys with a giant magnetocaloric effect for magnetic refrigeration from ~20 to ~290 K. *Appl. Phys. Lett* **70,** 3299 (1997).
8. Singh, N. K. *et al.* Itinerant electron metamagnetism and magnetocaloric effect in RCo$_2$-based Laves phase compounds. *J. Magn. Magn. Mater.* **317,** 68 (2007).
9. Gratz, Z. & Markosyan, A. S. Physical properties of RCo2 Laves phases. *J. Phys.: Condens. Matter* **13,** R385 (2001).
10. Zhong, W., Au, C. K. & Du, Y. W. Review of magnetocaloric effect in perovskite-type oxides. *Chin. Phys. B* **22,** 057501 (2013).
11. Phan, M. H. & Yu, S. C. Review of the magnetocaloric effect in manganite materials. *J. Magn. Magn. Mater. 308* 325 (2007).
12. Liu, J. Optimizing and fabricating magnetocaloric materials. *Chin. Phys. B* **23,** 047503 (2014).
13. Hu, F. X., Shen, B. G. & Sun, J. R. Magnetic entropy change involving martensitic transition in NiMn-based Heusler alloys. *Chin. Phys. B* **22,** 037505 (2013).
14. Hu, F. X. *et al.* Influence of negative lattice expansion and metamagnetic transition on magnetic entropy change in the compound LaFe$_{11.4}$Si$_{1.6}$. *Appl. Phys. Lett.* **78,** 3675 (2001).
15. Hu, F. X., Shen, B. G., Sun, J. R. & Wu, G. H. Large magnetic entropy change in a Heusler alloy Ni$_{52.6}$ Mn$_{23.1}$ Ga$_{24.3}$ single crystal. *Phys. Rev. B* **64,** 132412 (2000).
16. Liu, J. *et al.* Giant magnetocaloric effect driven by structural transitions. *Nat. Mater* **11,** 620 (2012).
17. Tegus, O., Brück, E., Buschow, K. H. J. & de Boer, F. R. Transition-metal-based magnetic refrigerants for room-temperature applications. *Nature* **415,** 150 (2002).
18. Wada, H. & Tanabe, Y. Giant magnetocaloric effect of MnAs$_{1-x}$Sb$_x$. *Appl. Phys. Lett.* **79,** 3302 (2001).

19. Yue, M., Zhang, H. G., Liu, D. M. & Zhang, J. X. MnFe(PGe) compounds: Preparation, structural evolution and magnetocaloric effects *Chin. Phys. B* **24,** 017505 (2015).
20. Hu, F. X. *et al.* Very large magnetic entropy change near room temperature in LaFe$_{11.2}$Co$_{0.7}$Si$_{1.1}$. *Appl. Phys. Lett.* **80,** 826 (2002).
21. Shen, B. G. *et al.* Recent progress in exploring magnetocaloric materials. *Adv. Mate.* **21,** 4545 (2009).
22. Shen, B. G., Hu, F. X., Dong, Q. Y. & Sun, J. R. Magnetic properties and magnetocaloric effects in NaZn$_{13}$-type La(Fe, Al)$_{13}$-based compounds. *Chin. Phys. B* **22,** 017502 (2013).
23. Fujita, A., Fujieda, S., Hasegawa, Y. & Fukamichi, K. Itinerant-electron metamagnetic transition and large magnetocaloric effects in La(Fe$_x$Si$_{1-x}$)$_{13}$ compounds and their hydrides. *Phys. Rev. B* **67,** 104416 (2003).
24. Zhang, H. & Shen, B. G. Magnetocaloric effects in *RTX* intermetallic compounds (R = Gd-Tm, T = Fe-Cu and Pd, X = Al and Si). *Chin. Phys. B* **24,** 127504 (2015).
25. Franco, V., Blazquez, J. S., Ingale, B. & Conde, A. The Magnetocaloric Effect and Magnetic Refrigeration Near Room Temperature: Materials and Models. *Ann. Rev. Mater. Res.* **42,** 305 (2012).
26. Li, L. W. *et al.* Two successive magnetic transitions induced large refrigerant capacity in HoPdIn compound. *Appl. Phys. Lett.* **103,** 222405 (2013).
27. Li, L. W. *et al.* Giant low field magnetocaloric effect and field-induced metamagnetic transition in TmZn. *Appl. Phys. Lett.* **107,** 132401 (2015).
28. Li, L. W. *et al.* Giant reversible magnetocaloric effect in ErMn$_2$Si$_2$ compound with a second order magnetic phase transition *Appl. Phys. Lett.* **100,** 152403 (2012).
29. Li, L. W. Review of magnetic properties and magnetocaloric effect in the intermetallic compounds of rare earth with low boiling point metals. *Chin. Phys. B* **25,** 037502 (2016).
30. Zhang, Y. K. *et al.* Magnetic properties and magnetocaloric effect in TmZnAl and TmAgAl compounds. *J. Alloys Compd.* **656,** 635 (2016).
31. Morikawa, T. & Wada, H. Effect of deviation from stoichiometry on magnetic and magnetocaloric properties in MnAs$_{1-x}$Sb$_x$. *J. Magn. Magn. Mater.* **272–276,** E583 (2004).
32. Cam Thanh, D. T. *et al.* Structure, magnetism, and magnetocaloric properties of MnFeP$_{1-x}$Si$_x$ compounds. *J. Appl. Phys.* **103,** 07B318 (2008).
33. Kuz'min, M. D. Factors limiting the operation frequency of magnetic refrigerators. *Appl. Phys. Lett.* **90,** 251916 (2007).
34. Lyubina, J. *et al.* Novel design of La(Fe, Si)$_{13}$ alloys towards high magnetic refrigeration performance. *Adv. Mater.* **22,** 3735 (2010).
35. Moore, J. D. *et al.* Reducing the operational magnetic field in the prototype magnetocaloric system Gd$_5$Ge$_4$ by approaching the single cluster size limit. *Appl. Phys. Lett.* **88,** 072501 (2006).
36. Morrison, K. *et al.* Capturing first- and second-order behavior in magnetocaloric CoMnSi$_{0.92}$Ge$_{0.08}$. *Phys. Rev. B* **79,** 134408 (2009).
37. Moore, J. D. *et al.* Reducing extrinsic hysteresis in first-order La(Fe, Co, Si)$_{13}$ magnetocaloric systems. *Appl. Phys. Lett* **95,** 252504 (2009).
38. Gutfleisch, O., Yan, A. & Müller, K. H. Large magnetocaloric effect in melt-spun LaFe$_{13-x}$Si$_x$. *J. Appl. Phys.* **97,** 10M035 (2005).
39. Lyubina, J., Gutfleisch, O., Kuzin, M. D. & Richter, M. La (Fe, Si)$_{13}$-based magnetic refrigerants obtained by novel processing routes. *J. Magn. Magn. Mater* **321,** 3571 (2009).
40. Yan, A., Müller, K. H., Schultz, L. & Gutfleisch, O. Magnetic entropy change in melt-spun MnFePGe (invited). *J. Appl. Phys.* **99,** 08K903 (2006).
41. Provenzano, V., Shapiro, A. J. & Shull, R. D. Reduction of hysteresis losses in the magnetic refrigerant Gd$_5$Ge$_2$Si$_2$ by the addition of iron. *Nature* **429,** 853 (2004).
42. Tan, X. Y., Chai, P., Thompson, C. M. & Shatruk, M. Magnetocaloric Effect in AlFe$_2$B$_2$: Toward Magnetic Refrigerants from Earth-Abundant Elements. *J. Am. Chem. Soc.* **135,** 9553 (2013).
43. Uhl, E. & Boller, H. The magnetic properties and anisotropy of the linear chain compound TlFe$_3$Te$_3$. *J. Phys. Chem. Solids.* **45,** 33 (1984).
44. Pelizzone, M. *et al.* First-order phase transition to strongly anisotropic ferromagnetism in Tl$_2$Fe$_6$Te$_6$. *J. Magn. Magn. Mater.* **42,** 167 (1984).
45. Lyubina, J., Hannemann, U., Cohen, L. F. & Ryan, M. P. Novel La(Fe, Si)$_{13}$/Cu Composites for Magnetic Cooling. *Adv. Energy Mater.* **2,** 1323 (2012).
46. Banerjee, S. K. On a generalised approach to first and second order magnetic transition. *Phys. Lett.* **12,** 16 (1964).
47. Defay, E. *et al.* The Electrocaloric Efficiency of Ceramic and Polymer Films. *Adv. Mater.* **25,** 3337 (2013).
48. Moya, X., Defay E., Heine V. & Mathur N. D. Too cool to work. *Nature Phys.* **11,** 202 (2015).
49. Zou, J. D., Shen, B. G. & Sun, J. R. Magnetic properties and magnetocaloric effect in TbCo$_{2-x}$Fe$_x$ compounds. *Chin. Phys.* **16,** 3843 (2007).
50. Tencé, S. & Chevalier, B. Magnetic and magnetocaloric properties of Gd$_2$In$_{0.8}$X$_{0.2}$ compounds (X = Al, Ga, Sn, Pb). *J. Magn. Magn. Mater.* **399,** 46 (2016).
51. Morellon, L. *et al.* Magnetocaloric effect in Tb$_5$(Si$_x$Ge$_{1-x}$)$_4$. *Appl. Phys. Lett.* **79,** 1318 (2001).
52. Liu, X. B., Altounian, Z. & Beath, A. D. Structure and magnetocaloric effect in the pseudobinary system LaFe$_{11}$Si$_2$ LaFe$_{11}$Al$_2$. *J. Appl. Phys.* **95,** 6924 (2004).
53. Krenke, T. *et al.* Magnetic superelasticity and inverse magnetocaloric effect in Ni-Mn-In. *Phys. Rev. B* **75,** 104414 (2007).
54. Krenke, T. *et al.* Inverse magnetocaloric effect in ferromagnetic Ni-Mn-Sn alloys. *Nat. Mat.* **4,** 450 (2005).

Acknowledgements

Author Contributions

M.F. and Q.M. designed the study, analyzed the data and wrote the paper. Q.M. synthesized the samples and did the transport measurements with J.Y., H.W. and R.K.; J.D. collected, processed and refined the X-ray data; Y.Z., B.X. and Q.C. did the magnetization measurements. All authors discussed the results and commented on the manuscript.

Additional Information

Competing financial interests: The authors declare no competing financial interests.

How to cite this article: Mao, Q. *et al.* Large low field magnetocaloric effect in first-order phase transition compound TlFe$_3$Te$_3$ with low-level hysteresis. *Sci. Rep.* **6,** 34235; doi: 10.1038/srep34235 (2016).